NAG1-519
IN-35-CR
217296

THEORY AND APPLICATIONS OF OPTICAL FIBER LEVER SENSORS

F. W. Cuomo

University of Rhode Island, Kingston, RI 02881-0817, USA

This paper illustrates the evolution of optical fiber lever concepts leading to several designs found useful in air and water applications. In particular, this technology has led to the development of underwater detectors of the pressure and pressure gradient kind. In addition an optical microphone with features not found in condenser microphones has been utilized in the measurement of pressure fluctuations in high speed boundary layers requiring sensors of small size, extended bandwidth, wide dynamic range, and high temperature capability. Finally similar concepts have been applied to the design of scale model acoustic arrays intended for acoustic imaging applications in the megahertz frequency range.

(NASA-CR-185344) THEORY AND APPLICATIONS OF OPTICAL FIBER LEVER SENSORS (Rhode Island Univ.) 22 p CSCL 14B
G3/35 Unclas 0217296
N89-26201

INTRODUCTION

Sensors based on a wide range of transductance mechanisms can be characterized as amplitude sensors. Any transduction method which produces a change in optical intensity proportional to an applied signal can be classified as such a sensor. Among this class of sensors, it is possible to differentiate between two types. The first comprises a conditioned light input signal passing through some form of acousto-optical interaction region where the light beam is amplitude-modulated by the surrounding field and then detected upon transmission. The second type, although similar in concept, detects its ensuing modulations upon reflection within the interaction region. This latter approach falls within the nomenclature of fiber optic levers. By definition, a fiber optic lever consists of a light beam conveyed to a vibrating target by a method that causes the power in the reflected beam to be modulated in a manner proportional to the target displacement. It is possible to describe three sensor concepts falling in this category. The first, shown in Figure 1(a), consists of a transmit fiber and at least one adjacent receive fiber. A minute motion of the reflector is translated into an optical power modulation ΔP at the photodetector. The second type, shown in Figure 1(b), is similar to the first but utilizes only one fiber and a fiber optic coupler to provide the change in optical output. The third approach, shown in Figure 1(c), utilizes a Fabry-Perot cavity at the distal end of the transmit fiber. In this case, both ends of the cavity are partial reflectors, and changes in the cavity length caused by an external field are translated into optical modulations by means of fringes generated at the output. The analytical implications associated with these concepts will be briefly reviewed next;

however, in this paper, we will concentrate on the approach shown in Figure 1(a).

THEORY

In most applications, the detection threshold is a viable parameter for sensor comparisons. A normalized modulation index defined by [1]

$$Q = \frac{1}{P_0} \frac{\Delta P}{\Delta p} \ (Pa^{-1}) \tag{1}$$

is a parameter which applies to any optical sensor. P_0 is the optical power at the output, ΔP is the induced change in optical power, while Δp is the unit change in pressure. The modulation index is used to calculate the sensor response and the minimum detectable threshold. The sensor response S is the differential voltage for a unit change in pressure

$$S = qP_0RQ \ (volts/Pa) \tag{2}$$

where q is the detector responsivity in ampere/watt, and R is the detector load resistance in ohms. Similarly the shot noise limited detection threshold can be written as

$$\Delta p_{(min)} = \frac{1}{Q} \left(\frac{2eB}{qP_0}\right)^{1/2} (Pa) \tag{3}$$

where e is the electronic charge in coulombs and B is the detection bandwidth in Hertz.

Multi-fiber lever

Eq. (1) can be used to represent the normalized modulation index Q of the optical fiber lever shown in Figure 1(a). In addition, it is possible to define a similar quantity Q^* given by

$$Q^* = \frac{1}{P_0} \frac{\Delta P}{\Delta D} \tag{4}$$

where ΔD becomes the change in gap between the distal end of the transmit/receive fibers and the reflector due to an external pressure field Δp acting upon it. From Eqs. (1), (2) and (4), it is possible to derive an expression for the sensor response

$$S = qR \frac{\Delta P}{\Delta p} = qR \frac{\Delta P}{\Delta D} \frac{\Delta D}{\Delta p} \tag{5}$$

where $\frac{\Delta P}{\Delta D}$ represents the induced change in optical power realized by the reflector motion, while $\frac{\Delta D}{\Delta p}$ relates to the membrane motion due to an external pressure field. Since $\frac{\Delta P}{\Delta D} = Q^* P_0$, the sensor response can be written as

$$S = qRQ^{*}P_0 \frac{\Delta D}{\Delta p} \tag{6}$$

Finally, a viable expression for S can be derived based on the appropriate conditions assigned to the quantity $\frac{\Delta D}{\Delta p}$. If the reflector consists of a thin, stretched, undamped circular membrane fixed at its edge, such as found in a microphone design, then it is straightforward to show that the membrane displacement at its center is given by

$$y = \frac{a^2 p}{4T} \tag{7}$$

or

$$\frac{\Delta y}{\Delta p} = \frac{\Delta D}{\Delta p} = \frac{a^2}{4T} \tag{8}$$

where a is the membrane radius in meters and T is the membrane tension in newtons/meter. Thus the sensor response becomes

$$S = \frac{qRQ^{*}P_0 a^2}{4T} \tag{9}$$

Given that the above quantities are: $q = 0.5$ amperes/watt, $R = 10^6\ \Omega$, $Q^{*} = 10^4\ m^{-1}$, $P_0 = 10^{-4}$ watt, $a = 1.6 \times 10^{-3}$ m, and $T = 500$ newtons/m, one obtains 6.4×10^{-10} volts/μPa, or -184 dB re 1 volt/μPa. The fundamental frequency of the first resonance peak is given by

$$f_1 = \frac{2.405}{2\pi a} \sqrt{\frac{\overline{T}}{\rho_s}} \tag{10}$$

where ρ_s is the membrane surface density in kg/m^2. From the above example, utilizing a metallized mylar membrane 1.27×10^{-5} m thick yielding a surface density of 1.64×10^{-2} kg/m^2, the resonance frequency becomes about 42 kHz. The third quantity representing the minimum detectable pressure can be obtained from Eqs. (1) and (3):

$$\Delta p_{(min)} = \frac{1}{Q} \left(\frac{2eB}{qP_0}\right)^{1/2} = \frac{4T}{Q^{*}a^2} \left(\frac{2eB}{qP_0}\right)^{1/2} \tag{11}$$

Utilizing the same example this quantity becomes 3.125×10^3 μPa or 70 dB re 1 μPa. It should be noted that the above analysis is based on a uniangular optical beam profile. This assumption is not necessarily correct. In fact, the profile is basically Lambertian in nature. Figure 2 shows the results of an experiment performed utilizing a beam from a light emitting diode coupled into a 100 micron core optical fiber whose output end is placed 600 microns from an opaque screen. A computerized CCD camera is focused onto the screen as shown. Figure 3 illustrates the distribution of light on the screen. Thus, a more realistic analysis of the fiber optic lever should include this result. Present research on this topic accounts for the Lambertian profile, as well as sensitivity maximization of the optical sensor. To improve sensitivity with a minimum number of receive fibers, two approaches have been considered. The first is based on the output ratio of two or more receive fibers having different core diameters [2], while the second controls the diameter and position of the reflector for optimum performance [3]. Figure 4 shows preliminary results of these

approaches. In this figure, the quantity k defines the mirror dimensions referenced to the core radius of the transmit fiber, while Q^* and D remain as originally described.

Single fiber lever

As an alternate to the multi-fiber concept, a single fiber can be used as shown in Figure 1(b). Eqs. (1), (2) and (3) apply also to this case, and calculations which include the coupler loss predict sensitivities equivalent to the arrangement of Figure 1(a). However, to achieve similar results, the fiber gap must be kept small.

Fabry-Perot cavity

The arrangement of Figure 1(c) is somewhat more complex but predicts improved sensitivities. The analysis can be briefly explained from Figure 5. Consider a beam of coherent light of amplitude A normally incident on a partially reflective boundary a which is reflected and transmitted into media α and β as shown. The phase difference δ between the reflected rays equals $\frac{4\pi d}{\lambda}$, λ being the light wavelength. It is possible to show that the ratio $\frac{I_r}{I_i}$ of the incident and reflected light intensities is given by

$$\frac{I_r}{I_i} = \frac{(r_1-r_2)^2+4r_1r_2\sin^2\frac{\delta}{2}}{(1-r_1r_2)^2+4r_1r_2\sin^2\frac{\delta}{2}} \tag{12}$$

and

$$\frac{d}{d\delta}\left(\frac{I_r}{I_i}\right) = \frac{2r_1r_2(1-r_1^2)(1-r_2^2)\sin\delta}{[(1-r_1r_2)^2+4r_1r_2\sin^2\frac{\delta}{2}]^2} \tag{13}$$

where r_1 and r_2 are the reflection coefficients of boundaries a and b, respectively. If one defines the sensitivity of the cavity as

$$S^* = \frac{\Delta}{\Delta d}\left(\frac{I_r}{I_i}\right) \tag{14}$$

where:

$$\frac{\Delta}{\Delta d} = \frac{\Delta}{\Delta\delta}\frac{\Delta\delta}{\Delta d} = \frac{\Delta}{\Delta\delta}\left(\frac{4\pi}{\lambda}\right) \tag{15}$$

one obtains:

$$S^* = \frac{8\pi r_1r_2(1-r_1^2)(1-r_2^2)\sin\delta}{\lambda[(1-r_1r_2)^2+4r_1r_2\sin^2\delta/2]^2} \tag{16}$$

In this treatment, it is assumed that the medium of the cavity is air. It is relevant to note that for large displacements ($\Delta d \gg \lambda$) fringe counting is suitable, while for small displacements ($\Delta d \ll \lambda$) it is possible to utilize the slope of one fringe to obtain sensitivities about three orders of magnitude larger than the multi-fiber lever previously discussed.

APPLICATIONS

Fiber optic lever hydrophone

In the early stages of development, several acoustic devices utilizing fiber optic levers have been constructed and tested . They include some prototypes recently designed as well as others which were devised some years ago but never reported in the literature. Among them the interest focused on two major types, the first being a low-frequency pressure hydrophone and the second intended for low-frequency detection of the acoustic pressure gradient providing directivity. The intent of these investigations focused on the determination of the acoustic sensitivities, beam patterns, and noise floor levels; other relevant parameters such as operational frequency optimization, miniaturization, and depth dependence were left for future work. In this paper, we shall confine our discussion to the performance of a simple pressure hydrophone, shown in Figure 6, which was designed utilizing a commercially available fiber optic bundle 1 meter long, with random fiber distribution at the distal end [4]. The bundle was held in place by a cylindrical brass body. A small front surface mirror was cemented on a room-temperature-vulcanized silicone RTV window installed in a brass ring with fine threads. The optimum working distance prior to testing was chosen by a simple adjustment of the ring on the transducer body which was provided with suitable holes allowing air-backed as well as water-loaded conditions. This device was tested in an acoustic tank, and a standard LC-32 hydrophone was used for comparison measurements . The hydrophone was tested with air and water inside the transducer body. Figure 7 gives the frequency response obtained in the 100-1000 Hz range. The patterns given in Figure 8 illustrate the omnidirectional characteristics at low frequencies.

Pressure sensors in turbulent flow measurements

The measurement of mean velocities, forces, pressures, and shear stresses can provide useful information about transition, separation and turbulent friction in the study of fluid flow. In most cases, previous sensors have lacked some of the features necessary to satisfactorily establish the flow properties. This paper discusses the development of an optical fiber pressure sensor whose active dimensions, sensitivity and frequency response have shown to improve the measuring capabilities presently available. This effort led to the construction of several flush-mounted devices utilizing active elements consisting of 1/2 mil metallized mylar and optically clear elastomers with a reflector attached. Figures 9(a) and 9(b) show the probe construction and the sensor design, respectively. This particular arrangement used stretched mylar with the specifications indicated on the Figure. These sensors were tested utilizing a 7" x 11" low-speed wind tunnel. A calibrated B & K type 4144 microphone was used to obtain comparison type data. A narrow band analysis derived from FTT runs at 250 Hz indicated that signals down to 60 dB re 20 μPa could be detected. Since these measurements were generally limited by the amplifier noise, a lower detectability is predicted with improved instrumentation. Figure 10 shows in non-

dimensionalized form some results obtained with the fiber optic sensor and compares it to published data on the behavior of piezoelectric transducers. Reference [5] provides a detailed description of this effort. The rationale which led to the utilization of optical fibers in turbulent boundary layer pressure measurements was stimulated by several promising factors associated with their implementation. First, the elimination of electromagnetic interference (EMI) and the passive characteristics of the device (absence of power requirements at the distal end of the fiber bundle) predict superior performance in comparison to other sensors such as the condenser microphone. In addition, design versatility, small size, sensitivity, low cost, and relative ease of implementation become important aspects of this research. It is relevant to note that the use of optical fiber levers (intensity modulation) or interferometric techniques (phase modulation) requires that the distal end of the optical fiber probe in the detection region be coupled to the surrounding field in some form sensitive to pressure fluctuations.

Pressure fluctuations at high temperatures

The measurement of pressure fluctuations in a turbulent boundary layer confined to ambient temperatures allows the use of metallized mylar reflectors and organic-coated silica fibers. At elevated temperatures and harsh environments, such as found in hypersonic wind tunnels, the measurement of pressure in high-speed boundary layers poses very stringent requirements [6]. A summary of essential specifications for these measurements is given in Table 1. According to Reference [6], several potential advantages exist utilizing fiber optic sensors for high temperature operations in place of other devices. In particular, the recent availability of metal-coated optical fibers, which can operate at temperatures as high as 750° C with gold coatings, and the use of metal bodies and diaphragms make this application very attractive. Based on optical fiber information given in Table 1 and a nickel membrane with a radius of about 0.4 millimeters and a thickness of 25.4 microns, the expected frequency response of the device extends to about 210 kHz. This prediction accounts for effects due to thermal expansion at high temperatures, changes in the elastic modulus and a loss of bandwidth. A detailed description of a prototype pressure sensor useful in high temperature environments is given in Reference [6].

Fiber optic lever microphone

In many respects, the fiber optic lever microphone can be constructed very similar to the condenser microphone. The inherent advantages found in the first type include: **(a)** the absence of a preamplifier close to the device because of lack of loading effects, **(b)** the size of the sensor, **(c)** an increase in bandwidth, and **(d)** a 6 dB increase in response below resonance because the condenser microphone responds to the mean displacement of the membrane, while the fiber optic microphone responds to the displacement at the center. Another important aspect is associated with the membrane damping which in a condenser microphone is achieved by the use of a backplate. Similar designs have been incorporated in a fiber optic microphone [7, 8].

Figure 11 shows the theoretical microphone response of both types based on backplate configurations given in Figure 12. These results were derived in Reference [7] based on computations intended to achieve a proper damping for the fiber optic equivalent.

Scale model fiber optic acoustic arrays

Acoustic imaging studies of the scattered fields from an underwater target can improve the target's spatial characteristics and dynamics. This approach can be realized in a controlled testing environment by means of scale model acoustic arrays. Since in many instances, the dimensions of piezoceramic elements are too large for high-frequency operation, optical fiber sensors have been considered as viable substitutes in the design of miniature acoustic arrays. Figure 13 illustrates an idealized design of an acoustic array consisting of fiber optic lever elements similar in construction to those shown in Figure 9(a). Their overall dimensions are such that, if placed side by side in a square matrix as shown, they can provide amplitude and phase information at megahertz frequencies. At present, similar designs have been successfully built and tested in air. Future plans include in-water measurements utilizing a computer-controlled acoustic tank designed for high-frequency applications. Figure 14 shows a photograph of this experimental facility.

CONCLUSIONS

The theoretical approach in optical fiber lever sensor designs has been briefly presented with emphasis on calculations leading to sensor response and limited detection threshold. Several applications have been discussed for in-air and in-water use. The frequency range covers a bandwidth extending from D. C. to the megahertz region. Due to space limitations, some other applications have been omitted; namely, the utilization of similar devices for the measurement of shear stresses in a turbulent boundary layer [9] and the construction of an ultrasonic probe for 3-dimensional sound field visualization [10]. It has been found that these sensors can be very effective in a variety of pressure sensing techniques.

ACKNOWLEDGMENTS

The author wishes to recognize the very helpful contributions provided by Mr. Gang He, a doctoral candidate in the Department of Physics at The University of Rhode Island. The theoretical analysis of the fiber optic microphone by Dr. Andong Hu is also appreciated. The extensive support and guidance by Dr. Allan Zuckerwar of the NASA-Langley Research Center during several stages of the reported research has been valuable to the success of these endeavors.

REFERENCES

1. Giallorenzi, T. G., Bucaro, J. A., Dandridge, A., Siegel, G. H., Cole, J. H., Rashleigh, S. C. and Priest, R. G. IEEE J. Quantum Electron. (1982) QE-18 626-665

2. Cuomo, F. W. In: SPIE Technical Symposium Proceedings (1984) 478 28-32

3. He, G. and Cuomo, F. W. To be published

4. Cuomo, F. W. J. Acoust. Soc. Am. (1983) 73 1848-1857

5. Cuomo, F. W. NASA-Langley Research Center Final Report, University of Rhode Island (1987)

6. Zuckerwar, A. J. and Cuomo, F. W. The 13th International Congress on Instrumentation in Aerospace Simulation Facilities Proceedings. Göttingen, West Germany (9/18-21/89)

7. Zuckerwar, A. J. J. Acoust. Soc. Am. (1988) 83 Supplement 1

8. Hu, A. In: Dissertation, University of Rhode Island (1987)

9. Cuomo, F. W., Kidwell, R. S. and Hu, A. J. Acoust. Soc. Am. (1987) 81 Supplement 1

10. Cuomo, F. W. 12th Congress on Acoustics Proceedings. Toronto, Canada (1986)

TABLE 1. Summary of essential specifications for measurement of pressure fluctuations in hypersonic flow.

Small size	<0.02 in. (0.508 mm)
High temperature	2000° F (1093° C)
Frequency response	200 kHz
Dynamic Range	0.01-10 psi (130-190 dB re 20 μPa)

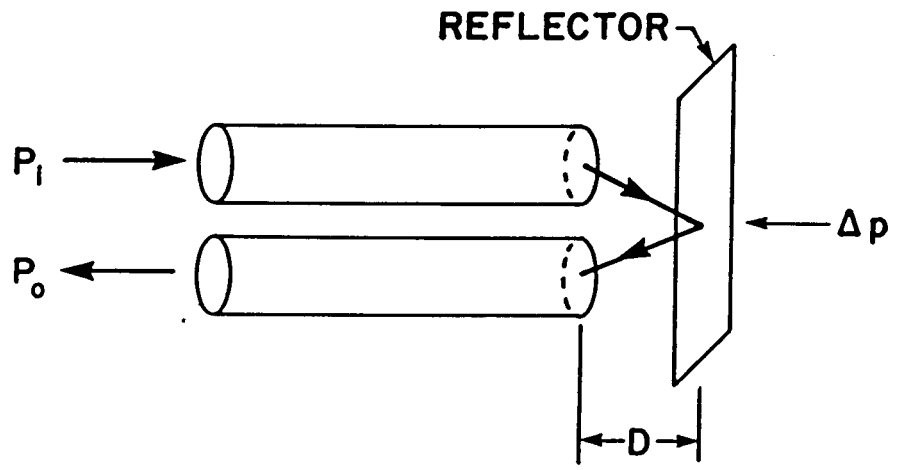

(a)

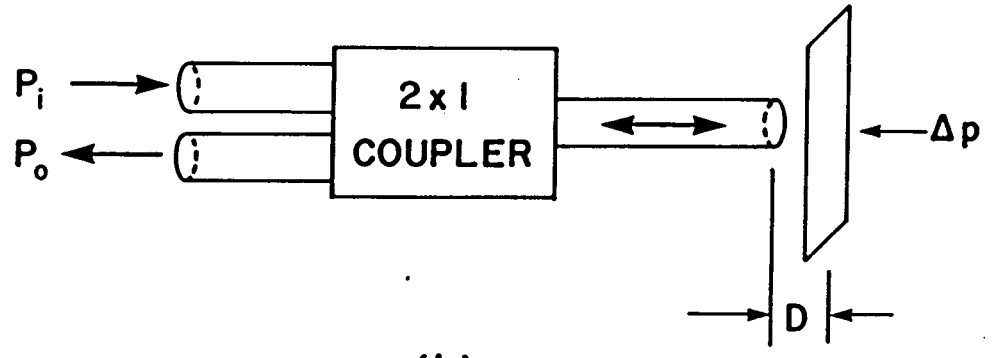

(b)

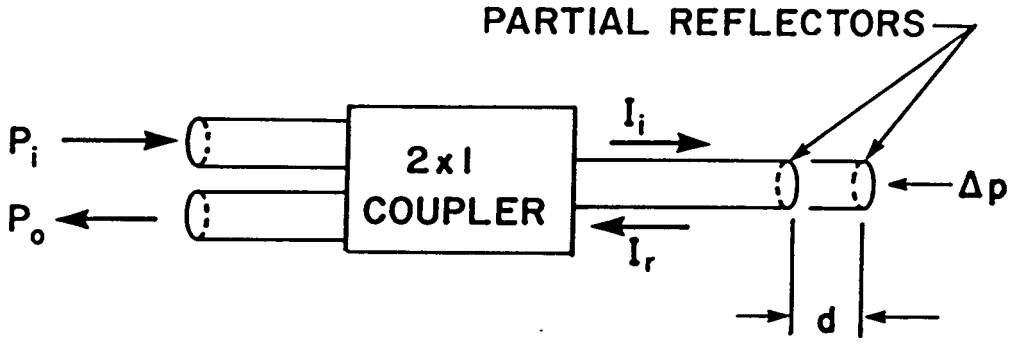

(c)

Figure 1.

SOME FIBER OPTIC LEVER CONFIGURATIONS

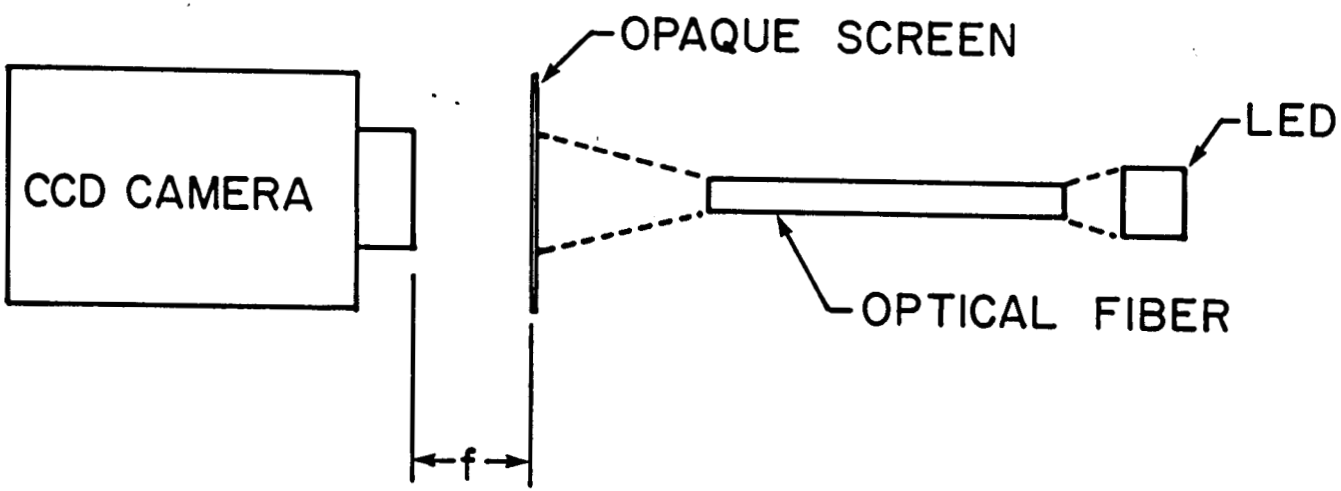

Figure 2.

EXPERIMENTAL SET-UP FOR BEAM PROFILE

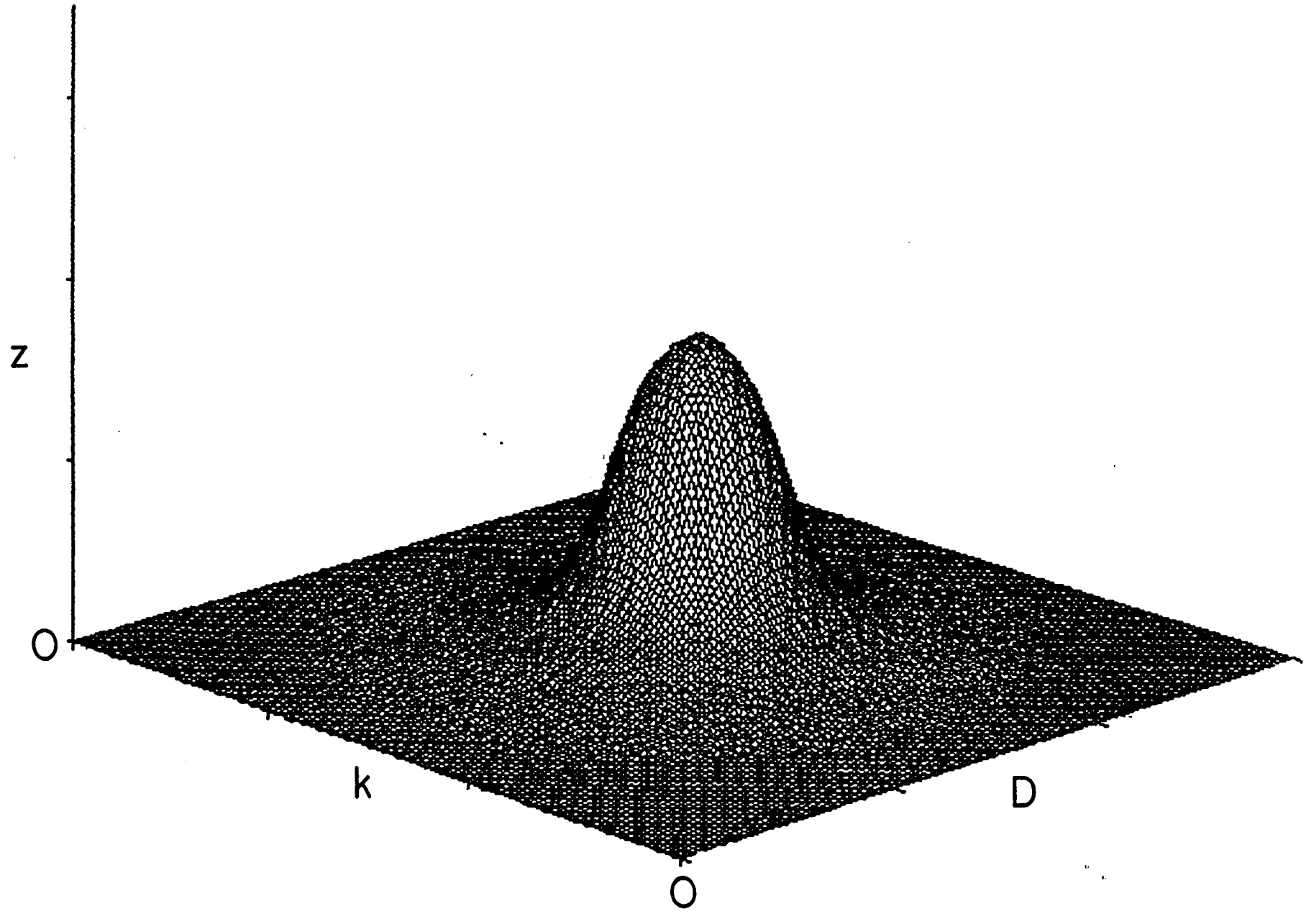

Figure 3.

BEAM PROFILE OF A 100 MICRON CORE FIBER, 600 MICRONS FROM SCREEN

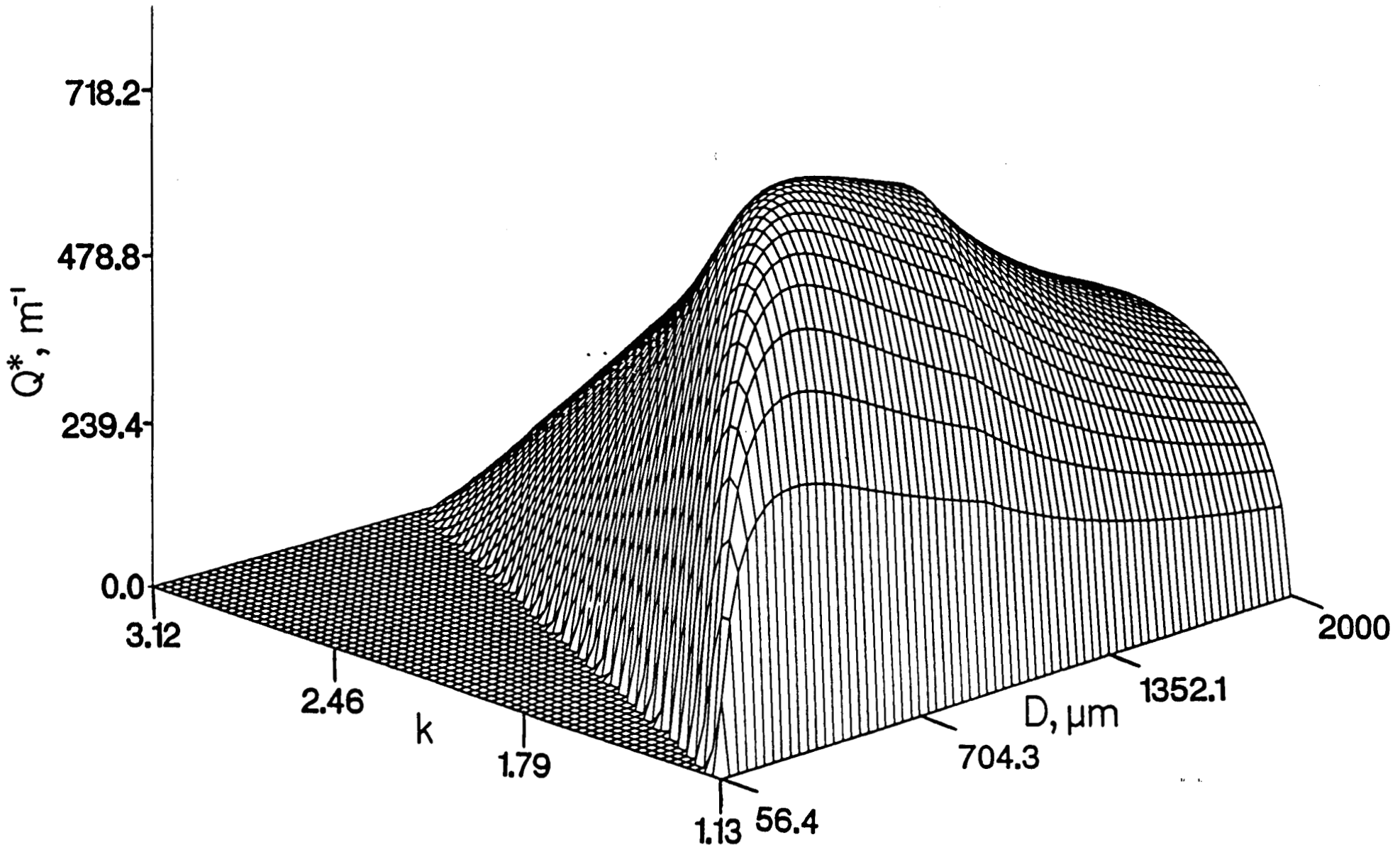

Figure 4.

THREE DIMENSIONAL REPRESENTATION OF Q*

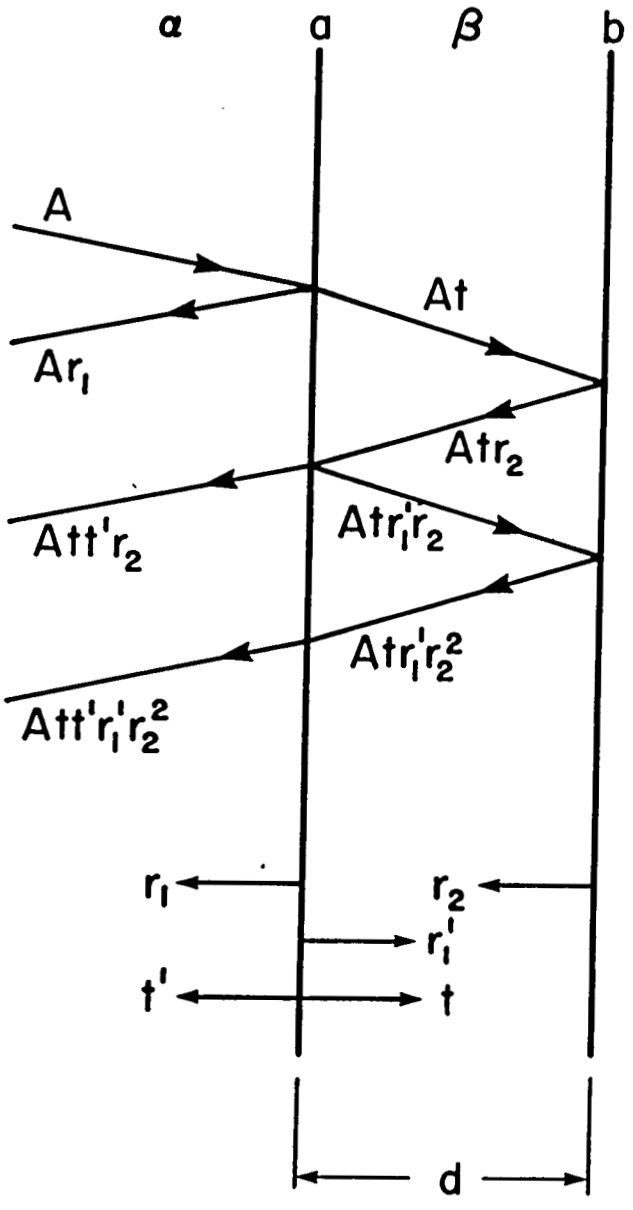

Figure 5.

FABRY-PEROT CAVITY

ORIGINAL PAGE IS
OF POOR QUALITY

Figure 6.
FIBER OPTIC LEVER PRESSURE HYDROPHONE

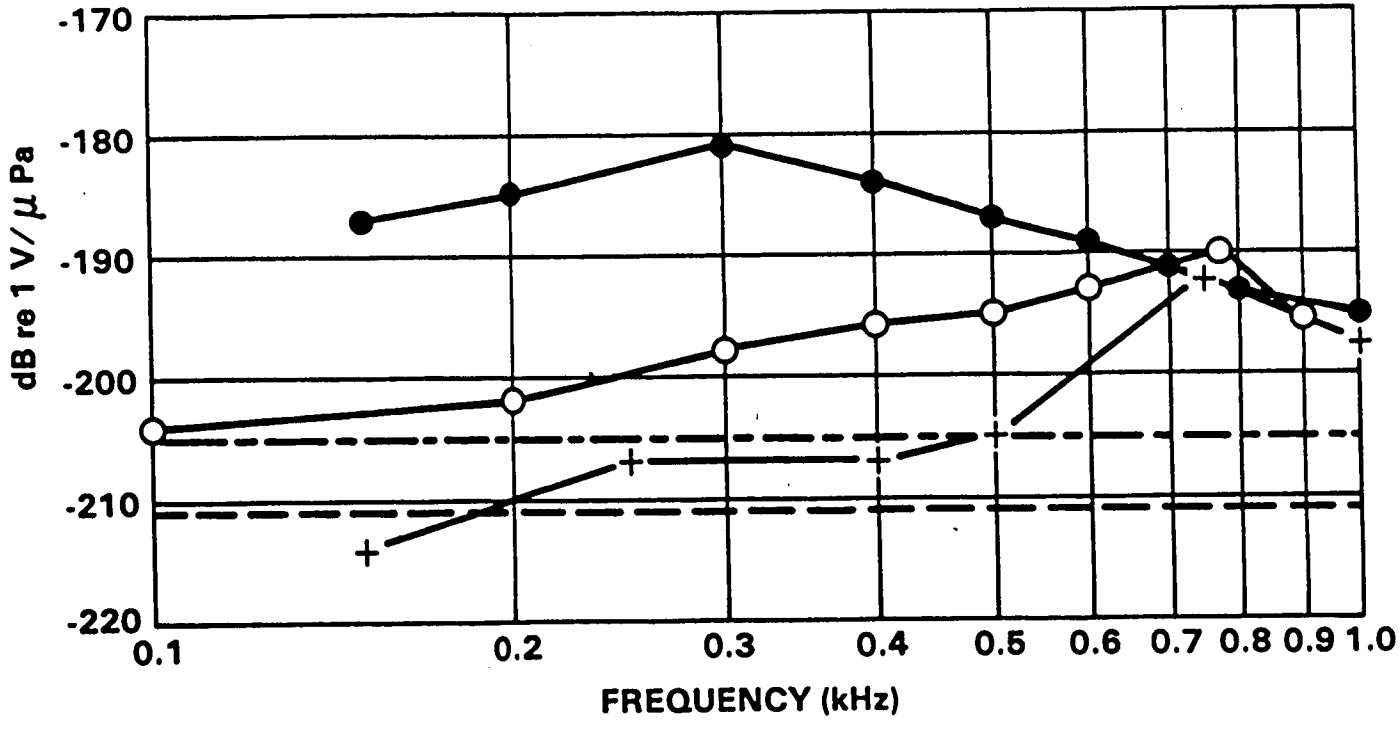

Figure 7.

OPEN CIRCUIT RECEIVING PRESSURE SENSITIVITY

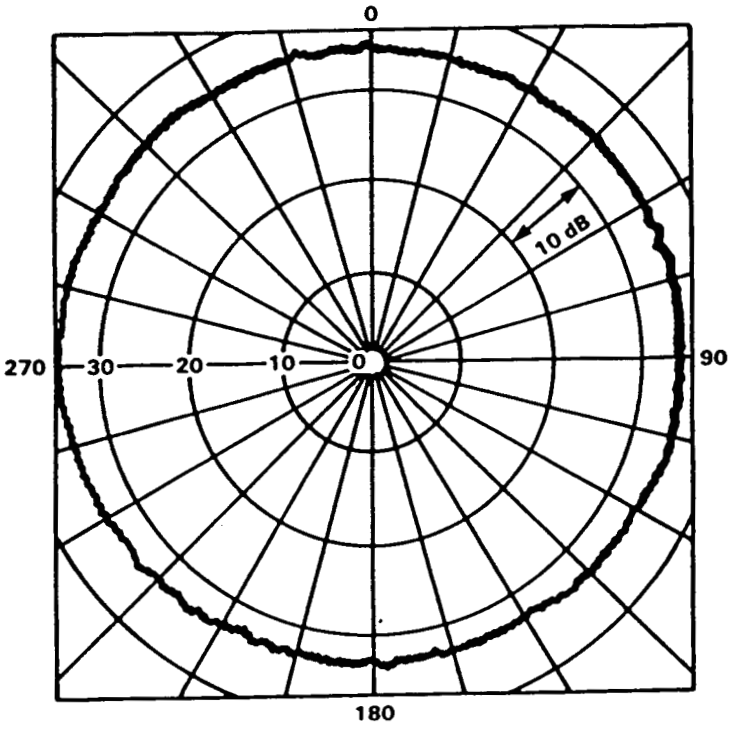

(A)
TRANSDUCER WATER-LOADED
FREQUENCY — 240 Hz
GATE — 3 ms

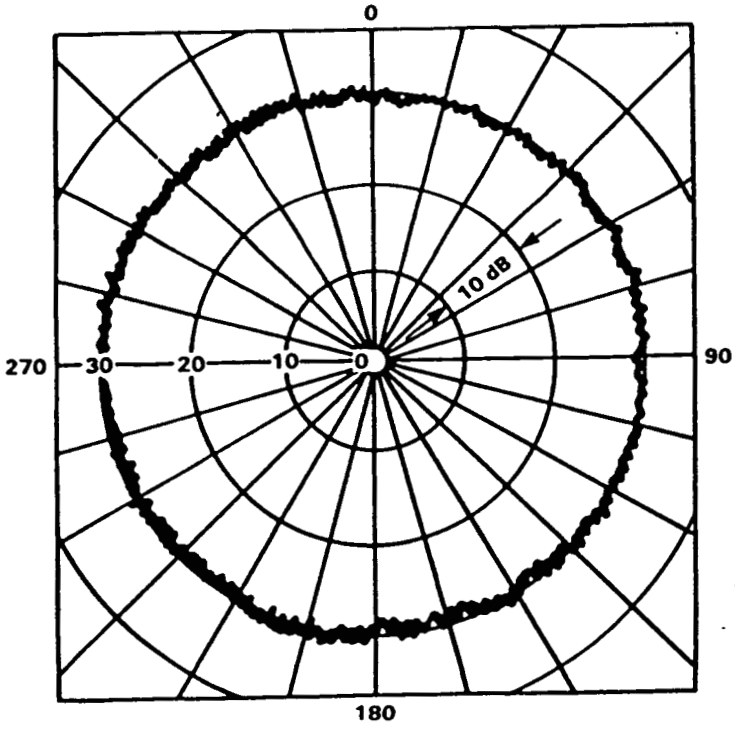

(B)
TRANSDUCER AIR-BACKED
FREQUENCY — 770 Hz
GATE — 3 ms

Figure 8.

DIRECTIVITY PATTERNS

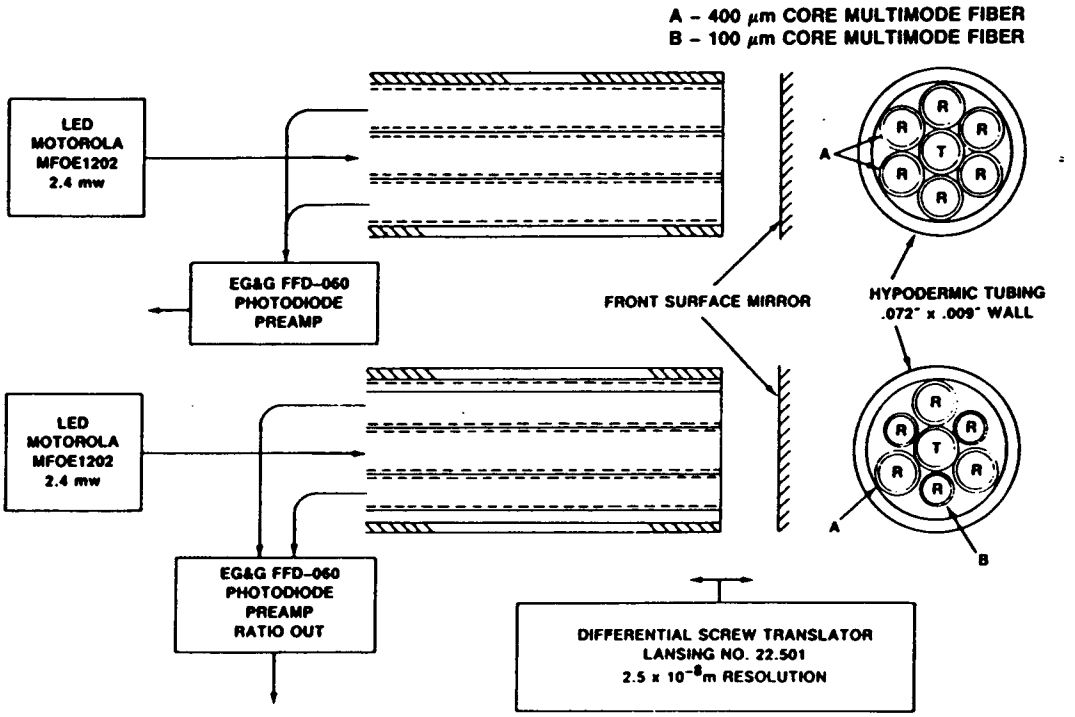

(a)

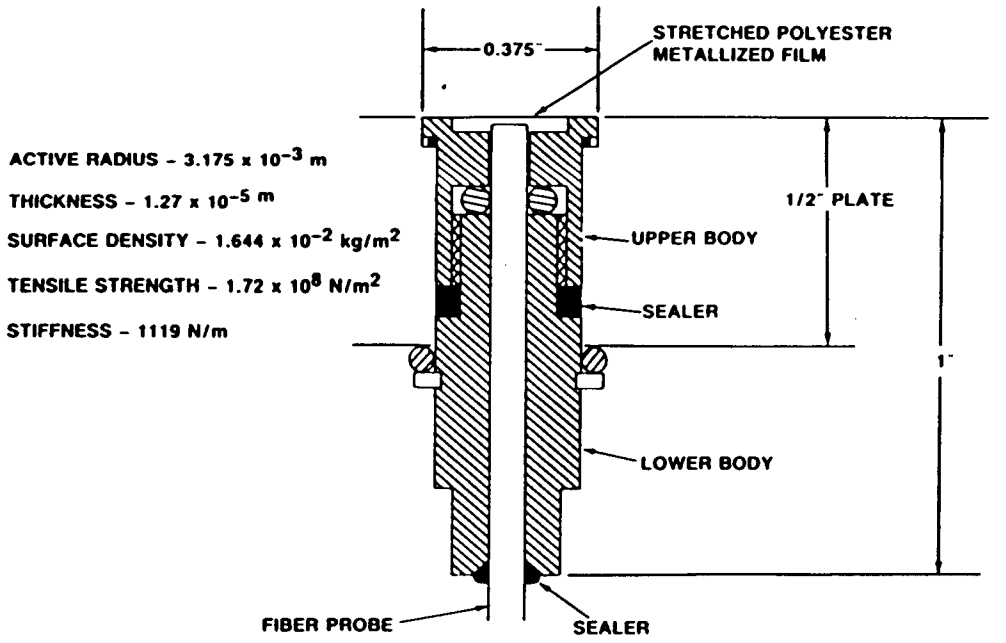

(b)

Figure 9.

OPTICAL FIBER PROBE CONSTRUCTION

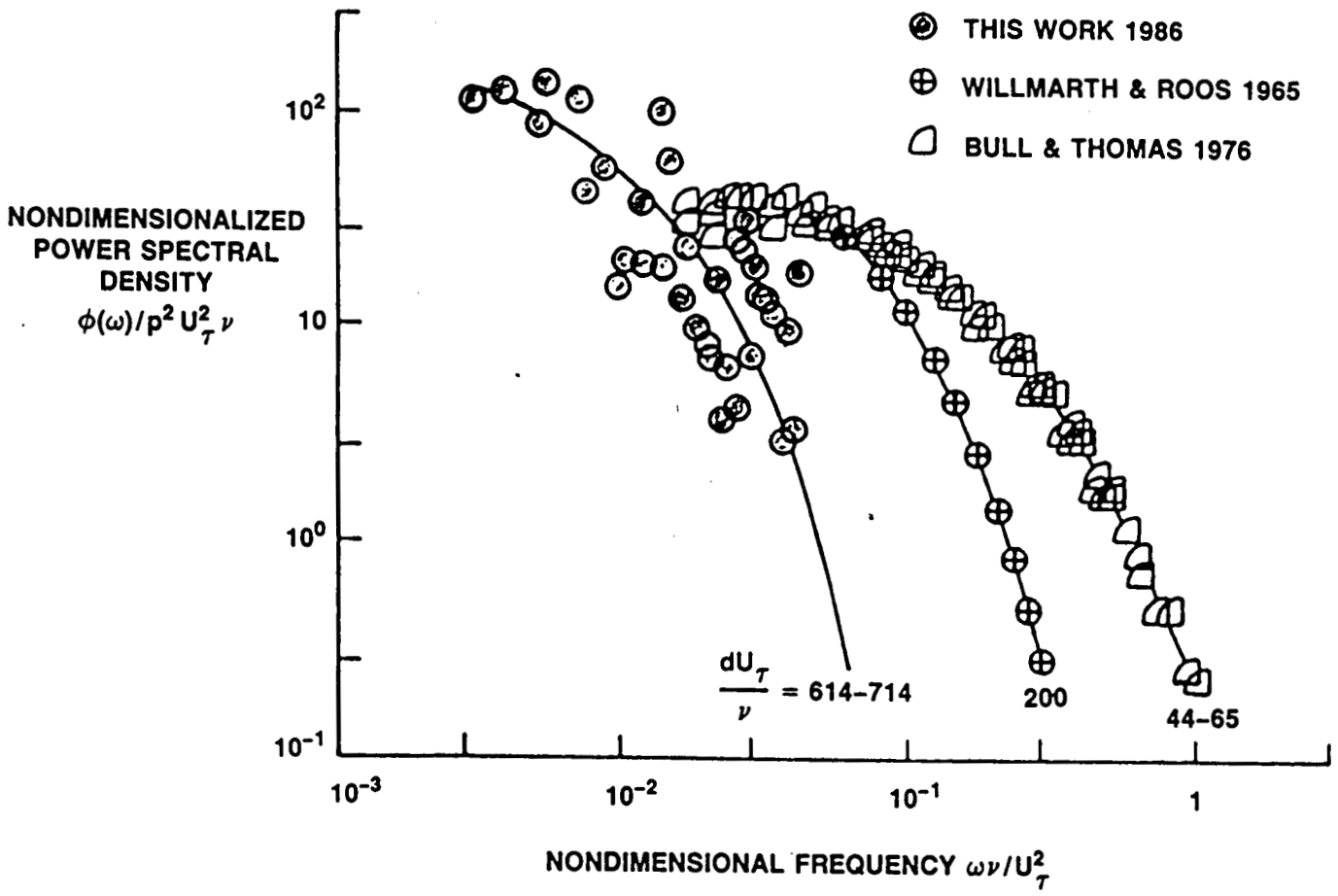

Figure 10.

POWER SPECTRUM OF WALL PRESSURE FLUCTUATIONS

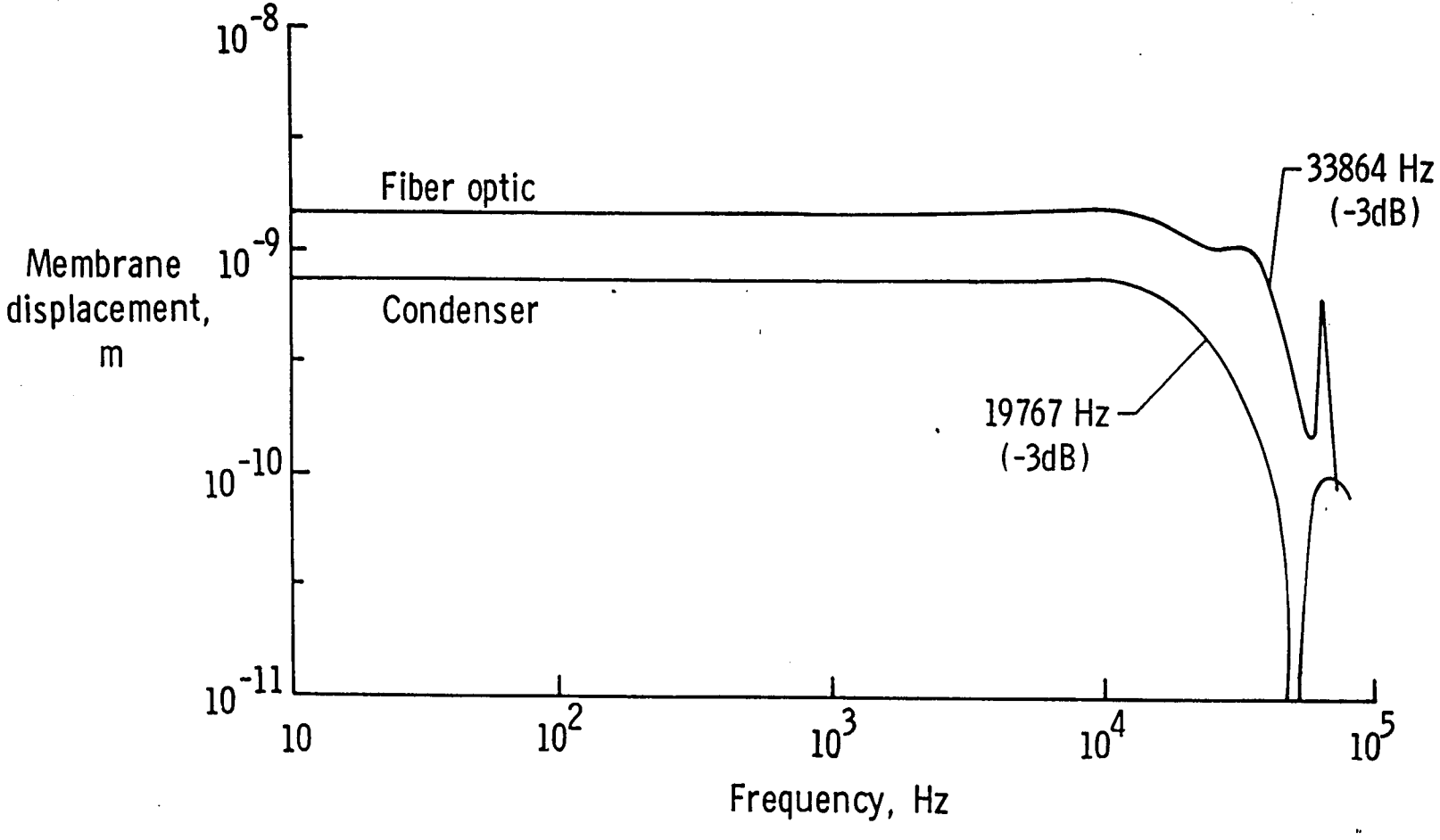

Figure 11.

THEORETICAL MICROPHONE RESPONSE RE 1 μPa - FIBER OPTIC VS. CONDENSER

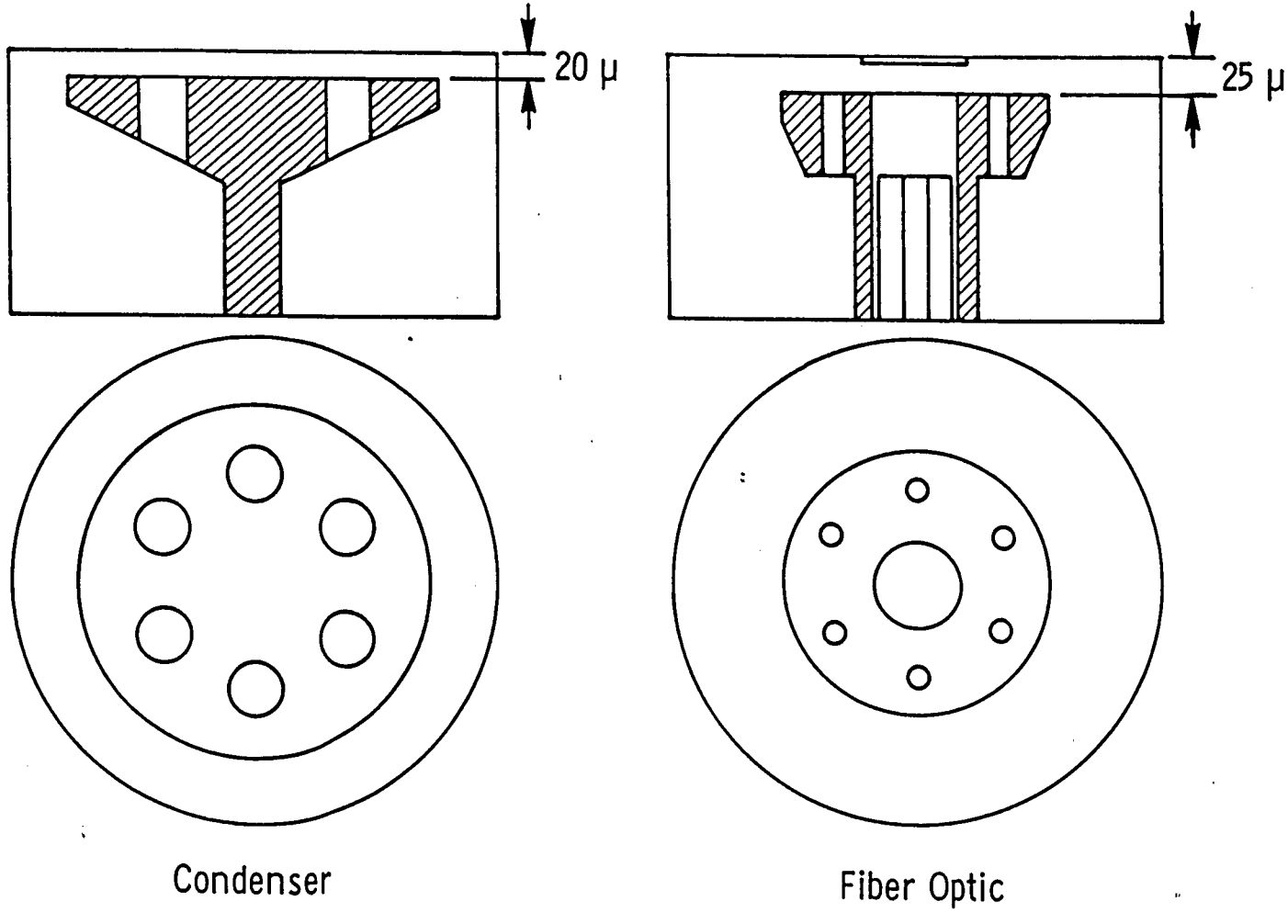

Figure 12.

BACKPLATE CONFIGURATION

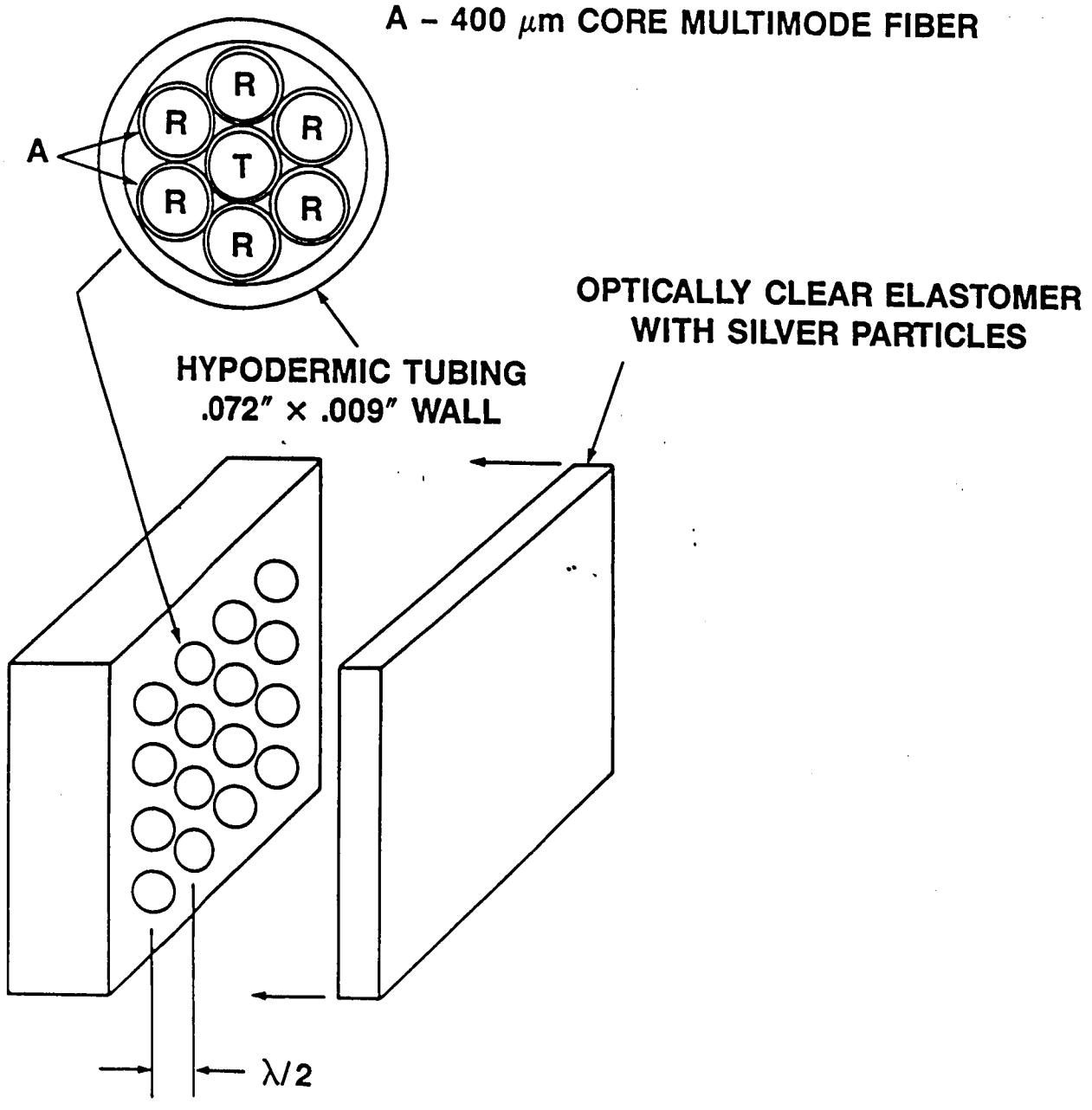

N0211-QA-89(N) 0849.4

Figure 13.
HIGH FREQUENCY ACOUSTIC ARRAY

ORIGINAL PAGE
BLACK AND WHITE PHOTOGRAPH

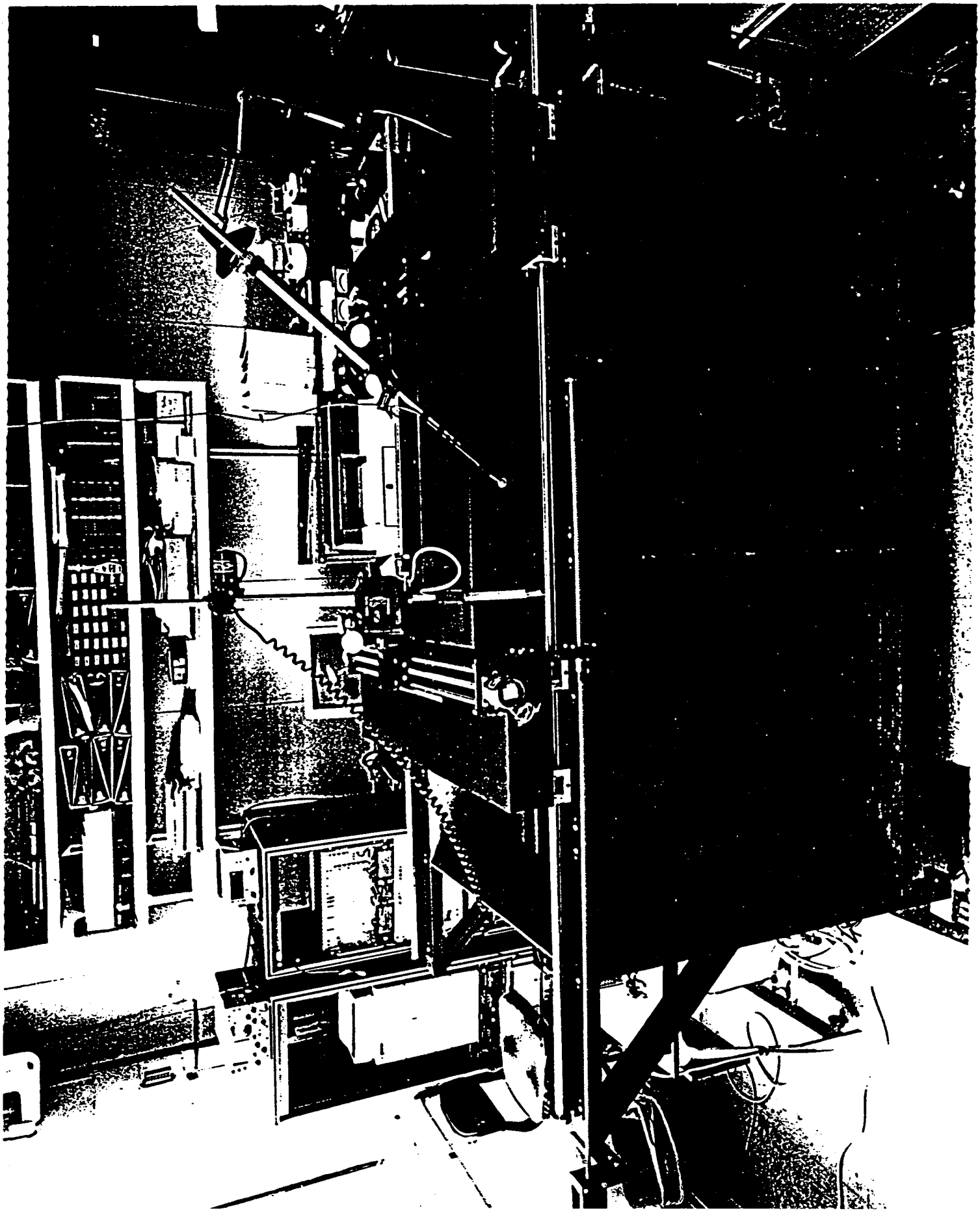

Figure 14.
HIGH FREQUENCY ACOUSTIC TANK